Iraqi Journal of Physics, 2025 *Vol.23, No4, PP.105-118*
https://doi.org/10.30723/ijp.v23i4.1400 *P-ISSN: 2070-4003*
E-ISSN: 2664-5548

Assessment of Heavy Elements Pollution and Environmental Impacts of the Severe Dust Storm in Iraq on May 2022

Rafah R. Ismail[1*], Saadiyah H. Halos[2], and Bushra Q. Al-Abudi[1]
[1]*Department of Astronomy and Space, College of Science, University of Baghdad, Baghdad, Iraq*
[2]*Atmosphere and Space Sciences Department, Space Research and Technology Center, Scientific Research Authority, Baghdad, Iraq*
[*]Corresponding author: rafah.ismail@sc.uobaghdad.edu.iq

Abstract
Dust storms frequent in Iraq can have far-reaching consequences for the distribution and abundance of heavy and trace elements within the soil, ultimately influencing the dynamics of ecosystems. This study aims to identify the sources of the severe dust storm in Iraq on May 16, 2022, and assess the heavy element pollution and their environmental impacts. The results revealed that the hybrid-single-particle-Lagrange-integrated trajectory (HYSPLIT) model trajectory of the dust storm agreed with MODIS visuals. The primary dust storm sources are identified as follows: the first source is from the shared border region between Syria (south of Rif-Dimasshq) and Jordan (north of Al-Ruwaished), and the second is from the northwestern area of Iraq, specifically north of Anbar and south of Nineveh. The dust samples mainly consist of clay, sand, and metals, according to particle size analyses, with sizes ranging from 6 nm to 50 µm and increasing the concentrations of trace elements, which affect the ecosystem and the possibility of changing soil properties and increasing the amounts of heavy metals that adversely affect the environment and human health. The contamination factor values showed very high pollution for the elements (Ni, Ge, Se, Mo, Ag, Cd, Sb, Te, I, Hg, and Bi). The I-geo index indicated it was extremely polluted with heavy elements (Ge, Te, I, Hg, Bi, and Se). Using the contamination factor values for the elements (Pb, Ni, Cd, Zn, Cu, Cr, Hg, and Fe), the pollution load index was found to be 2.68, indicating environmental pollution.

Article Info.

Keywords:
Dust Storms, Environmental Impacts, Pollution Indicators, Heavy Elements, Trace Elements.

Article history:
Received: Nov. 17, 2024
Revised: Jan. 22, 2025
Accepted: Feb.01, 2025
Published:Dec.01,2025

1. Introduction
Often, the natural environment is subject to the forces of wind and extreme weather events. There are intense dust storms in Iraq in a few months of the year. These atmospheric phenomena can have far-reaching consequences for the distribution and abundance of heavy and trace elements within the soil, ultimately influencing the dynamics of ecosystems. Understanding the mechanisms by which winds and dust storms affect the redistribution of these elements is crucial for assessing the environmental impacts and developing appropriate management strategies. Winds and dust storms can mobilise and transport soil particles containing heavy and trace elements, redistributing them across different landscapes [1]. The erosion of soils and the subsequent suspension of particulates in the air allows for the long-range transport of these elements, which can be deposited in new locations, sometimes far from their sources [2]. The extent of redistribution is influenced by various factors, including the intensity and duration of the wind or dust storm, the geochemical properties of the soil, and the specific characteristics of the heavy and trace elements involved [3]. Certain elements, such as Lead, Cadmium, and Mercury, may be more readily mobilized and transported due to their higher volatility or association with fine soil particles [4]. The redistribution of heavy and trace elements can have significant implications for the overall dynamics of ecosystems. These changes in element distribution can alter nutrient availability and cycling, affecting the growth and productivity of primary producers, such as plants and algae [5]. Moreover, the

introduction of elevated concentrations of toxic elements can pose risks to the health and survival of various organisms, potentially disrupting trophic interactions and food web structures. This trophic interaction can lead to shifts in species composition and community structure, ultimately affecting the overall biodiversity and resilience of the ecosystem [6]. In coastal and aquatic environments, the deposition of wind-borne elements can also influence water quality, sediment composition, and the bioavailability of elements to aquatic biota. These changes can cascade effects on the ecological functions and services these ecosystems provide [5].

Megatons of dust are released into the sky annually by intense winds that blow close to the earth's surface in the dry regions. Dust particles significantly impact the Earth's radiation balance by interacting with solar radiation and altering cloud properties [7]. Dust plays a crucial role in climate regulation by acting as condensation nuclei and influencing precipitation processes. The middle east region experiences frequent dust storms, with Northern, between the Tigris and Euphrates rivers and along the Syrian-Iraqi border being a significant dust emitter [8]. Dust storms occurring in the Middle East have connections to climate change. Human activities have accelerated the occurrence of dust storms, significantly impacting the climate and ecosystems. The origin of a dust storm can be identified by analyzing its mineralogical composition and the trajectories of the air masses. Dust mineral composition varies from one location to another due to atmospheric chemical reactions and the distance from the source region [9].

This study aims to identify the sources of the dust storm in Iraq on May 16, 2022, and assess the environmental impacts by characterizing and analyzing deposited dust samples using a set of devices and many indicators to assess the pollution caused by the dust storms.

2. Materials and Methods

This part describes the materials, tools, and equipment employed to achieve the study objectives and the systematic methods to carry out the work and to ensure reliable results.

2. 1. Trajectory Model

The backward trajectories of dust storms can be tracked for a specified duration utilizing the hybrid-single-particle-Lagrangian-integrated trajectory (HYSPLIT) model. The HYSPLIT, which was developed by the National Oceanic and Atmospheric Air Lab of the United States, has been used in extensive studies to model the distribution and movement of air pollutants. To model the movement of air parcels produced by wind advection, the HYSPLIT model uses meteorological data that is gridded geographically and temporally [10]. The model can locate the dust's source and follow the dust particles' course [11, 12]. A backward trajectory model was built to determine the dust storm's destination and the direction of its movement over the Middle East and Iraq. The models utilised the regular trajectories option based on data from the global data assimilation system (GDAS) at one-degree resolution. The tracking produces geographic information system (GIS) shape-file trajectories with 96 dots per inch (dpi) resolution.

2. 2. Sample Collected

This work collected a sample of deposited airborne dust during an intense dust storm on May 16, 2022, in Iraq. A sample of dust deposited on the roof of the University of Baghdad in the city of Baghdad (33°16'30.7"N, 44°22'48.1"E) was collected at an altitude about 50 meters above sea level. The work method was based on collecting amounts of dust deposited and transported during dust storms by setting up a plastic container 40 cm high and 60 cm in diameter with an open top to collect dust. The sample was carefully

emptied into a plastic clean tube from the dust container. It is then transferred to practical laboratories in the Scientific Research Authority / Directorate of Materials Research to analyses the geochemical composition, dust grain size, and determination of heavy and trace elements components in dust storm samples.

2. 3. Grain-Size Analysis

Scanning Electron Microscope (SEM) (TESCAN, Vega III/Czech Republic), was used to obtain high-resolution images that reveal the surface morphology, particle distribution, and bonding mechanisms [12]. The SEM is essential in all disciplines that need to characterize solid materials. It also precisely measures very small features and objects down to 50 nm in size. Analysis using SEM is considered to be "non-destructive"; that is, X-rays produced by electron interactions do not reduce the sample's volume, allowing for repeated analysis of the same materials [13].

Atomic force microscopy (AFM) is the most versatile and powerful microscopy technology for studying samples at the nanoscale. AFM enables 3D characterization of nanoparticles at sub-nanometer resolution, which offers many benefits compared to dynamic light scattering, electron microscopy, and optical characterisation techniques [14, 15]. The analysis was conducted to measure the smallest size fraction present in dust storms samples using AFM (molecular imaging scanning probe microscope, Model: PICOSPM, US).

An X-ray diffraction XRD (6000 / Shimadzu, Japan), is a device used to study the crystal structure of materials, providing insights into the mineralogical composition and the characterization of the soil composition which helps in understanding their properties. X-rays directed at a sample positioned along the axis of the spectrometer (goniometer) are diffracted by the sample. The variations in the diffracted X-ray intensity are quantified, documented, and graphed to the sample's rotation angles. The outcome is known as the sample's X-ray diffraction pattern. XRD analysis is used for multiple purposes, including: determining the composition and classification of crystals in materials to identify their structure, estimating the size and shape of crystal grains in materials and analyzing the composition of unknown materials by comparing peaks with a crystal database [16].

2. 4. Chemical and Mineralogical Analysis

In addition to XRD, which provides insights into the mineralogical composition and the characterization of the soil composition, one analytical method for determining the elemental composition of different materials is X-ray fluorescence spectrometry, which yields the same result. Nondestructive, multi-elemental, quick, and inexpensive are some of XRF's advantages. A beam of powerful X-rays is used to irradiate a sample. When the sample's excited electrons return to their ground states, they release X-rays specific to the elements present in the sample. The elements that can be studied and their detection levels are dependent mainly on the spectrometer equipment utilized by the SPECTRO XEPOS (ED-XRF) device, in which the concentration elemental range for XRF is from Sodium (Na) to Uranium (U) measured by parts-per-million (ppm) [17]. The behavior of atoms when they interact with radiation makes the analysis of major and trace elements in geological materials by X-ray fluorescence possible. The simplicity and affordability of sample preparation, combined with the stability and user-friendliness of X-ray spectrometers, make this approach one of the most prevalent for analyzing major and trace elements in rocks, minerals, and sediments [18].

Energy dispersive X-ray analysis (EDX or EDS) is an analytical technique used for a sample's elemental analysis or chemical characterization. Its characterization capabilities are mainly due to the fundamental principle that each element has a unique

atomic structure, allowing a unique set of peaks on its electromagnetic emission spectrum [19].

3. Pollution Indicators

The risks arising from pollution with heavy elements in the ecosystem require determining their concentrations in the dust deposited during the dust storm, by choosing the appropriate analytical method [20]. Several indicators can be used to evaluate the environmental impacts of dust storms.

3. 1. Contamination Factor

Contamination Factor (CF) assesses the presence of heavy metals in the soil at levels exceeding their normal abundance in the Earth's crust. It is an effective tool for observing heavy element contamination. The contamination factor in classifying the level of heavy element contamination in dust samples depends on dividing the dust's concentration of each element by the concentration of the natural abundance or natural background of that element. The CF can be calculated by using the following equation [21]:

$$\mathrm{CF} = \frac{\mathrm{Cm}_{(\mathrm{Sample})}}{\mathrm{Cm}_{(\mathrm{Background})}} \qquad (\mathbf{1})$$

where $\mathrm{Cm}_{(\mathrm{Sample})}$ is the element concentration in the sample., and $\mathrm{Cm}_{(\mathrm{Background})}$ is the background level of the element.

3. 2. Geo-accumulation index

The geo-accumulation index (I-geo) is one of the most widely used indicators for quantitatively measuring heavy element pollution by comparing the concentrations of heavy elements in a dust sample with the natural abundance of these elements in the earth's crust. This indicator determines the extent of the terrestrial factors on soil pollution. The I-geo index can be calculated using Eq. 2 [22]:

$$\mathrm{Igeo} = \log_2\left(\frac{\mathrm{Cn}_{\mathrm{Sample}}}{1.5 \times \mathrm{Bn}_{\mathrm{Background}}}\right) \qquad (\mathbf{2})$$

where $\mathrm{Cn}_{(\mathrm{Sample})}$ is the element concentration in the sample, and $\mathrm{Bn}_{(\mathrm{Background})}$ is the background level of the element. Many environmental studies use a correction factor of 1.5 to account for natural fluctuations in background element levels [22].

As illustrated in Table 1, the Contamination Factor is divided into four grades, while I-geo is categorized into seven grades.

Table 1: Contamination Factor and I-geo polluted grades.

CF range	Description	I-geo range	Description
CF<1	Low contamination factor	I-geo <0	Practically unpolluted
		0≤ I-geo <1	slightly polluted
1≤ CF<3	Moderate contamination factor	1≤ I-geo <2	Moderately polluted
		2≤ I-geo <3	moderately severely polluted
3≤ CF<6	Considerable contamination factor	3≤ I-geo <4	Severely polluted
		4≤ I-geo <5	Severely extremely polluted
6≤ CF	Very high contamination factor	5≤ I-geo	Extremely polluted

3. 3. Pollution Load Index

The Pollution Load Index (PLI) is used to assess the level of pollution in the environment by using the contamination factor index for many elements in a specific area and combining them into a single value, which facilitates comparing pollution between different locations and tracking changes in the level of pollution over time. It is calculated using the following equation [23]:

$$\mathrm{PLI} = \sqrt[n]{\mathrm{CF}_1 \times \mathrm{CF}_2 \times \mathrm{CF}_3 \ldots\ldots\ldots \mathrm{CF}_n} \qquad (\mathbf{3})$$

where *n* is number of elements.

If PLI < 1: indicates perfection
PLI = 1: indicates pollutants are present but only at baseline levels.
PLI > 1: indicates deterioration of site quality.

4. Results and Discussion

A dust survey is conducted to understand the spread of trace elements during storms to different areas. This helps identify any danger to the surrounding environment, especially Baghdad Governorate, during the period of climate transitions and observe the amount of dust saturated with trace elements. Many tests were conducted to determine the number of materials, their sizes, and their spread.

4. 1. Identification of Dust Storm Sources

HYSPLIT model was constructed to determine the backward trajectories, as shown in Fig. 5. The calculation of the route was carried out by the location time integration of the air expulsion through three-dimensional winds in the patterns ending at 11:00 UTC on May 16, 2022, with the interval of each path being 24 hours for the governorates (Baghdad, Wasit, and Karbala). The trajectories pattern was selected to analyze 50, 1000, and 1500 m above-ground levels.

The result of the HYSPLIT model for the pattern is displayed in Fig. 1. For the three altitudes of 50, 1000, and 1500 m on May 16, 2022, the likely primary sources of the dust in the studying region from the territorial states were the shared border region between both Syria (south of Rif-Dimasshq) and Jordan (north of Al-Ruwaished), in addition to a local source in the northwestern region of Iraq, specifically north of Anbar and south of Nineveh.

MODIS visuals of the study region are shown in Fig. 2 [24], showing that the dust storm on May 16, 2022, covered large regions of Iraq, Kuwait and Saudi Arabia in the south and Iran in the east; thus, MODIS observations established the output of the HYSPLIT model.

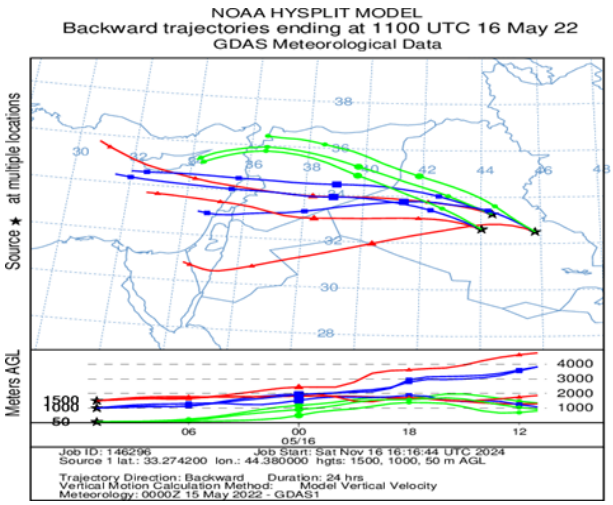

Figure 1: HYSPIT backward trajectories of a dust storm at 11:00 UTC.

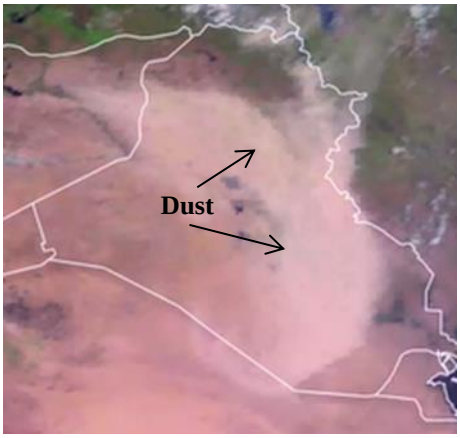

Figure 2: MODIS images for the case studies at 08:00 UTC 16 May 2022.

4. 2. Particle Size Analyses

Three images in Fig. 3 show details of the dust collected during the severe dust storm on 16/5/2022 using a Scanning Electron Microscope (SEM) in various magnifications (MAG). The dust storm sample in Fig. 3(a) shows that the particles were sharp-edged and generally irregular in shape and sizes, and subtle differences in structure, and other researchers have obtained similar results [25-27].

The results of the particle size analyses indicating that their sources are natural, such as sand from desert areas or eroded rocks in natural geological environments. The size of the particles ranges from 50 nm to 50 µm. The surface of the particles with small grains attached to them in Fig. 3 (b) indicates that the particles were exposed to a long transport process due to the accumulation of fine particles during their long transport in the atmosphere. The size of the visible particle's ranges from 5-10 µm, with fine grains up to 0.5 µm attached to the surface of the larger particles.

Fine grains attached to the surface of the large particles in different sizes and shapes that appeared clearly in Fig. 3 (c), indicate a mixture of different sources that may be natural, geological, or industrial. The sample was affected by natural, human, or industrial sources. The size of the particles ranges from 2-5 µm, while the size of the attached particles ranges from 0.05 - 1 µm. Particles smaller than 10 µm (PM10) and less than 2.5 µm (PM2.5) are fundamental in analyzing the environmental and health impact because they may penetrate the human respiratory system. In addition to very fine particles that

reach a size of 50 nm, these objects may be present in atmospheric dust due to natural weathering or from emissions from car or factory exhausts or combustion processes.

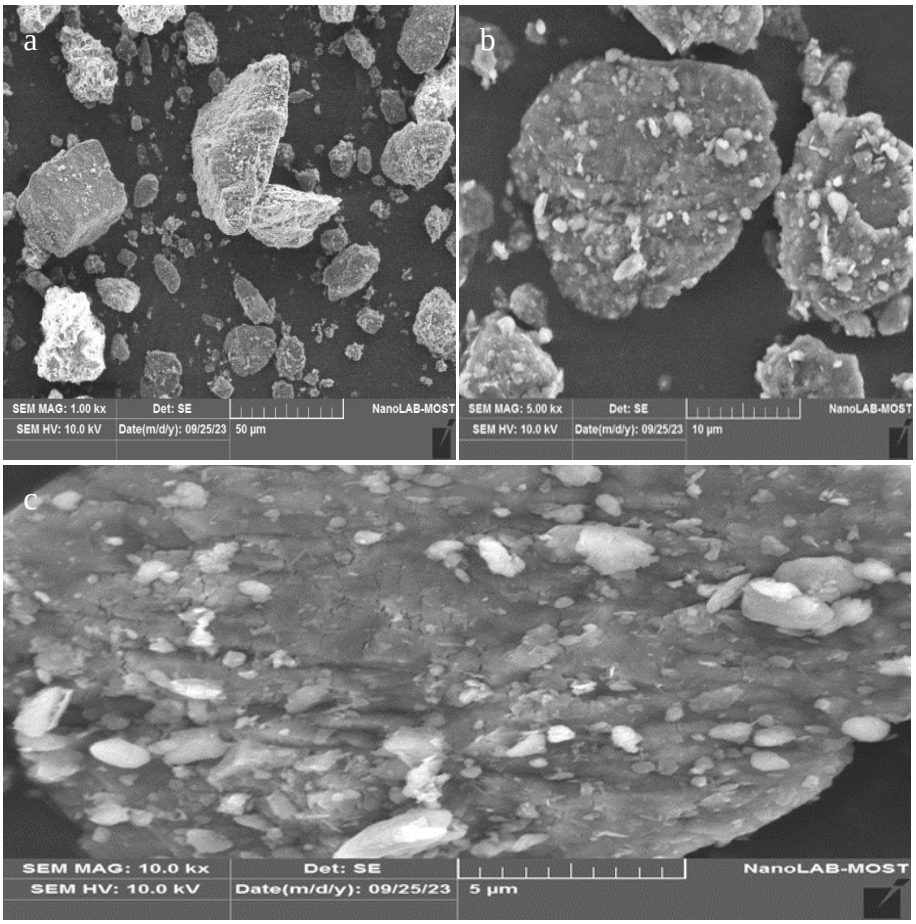

Figure 3: SEM images of the May 16, 2022 dust sample (a) 1000 MAG, (b) 5000 MAG, and (c) 10000 MAG.

Grain size analyses using the AFM image of the removed and collected dry dust during the dust storm in Baghdad Governorate on May 16, 2022, are illustrated in Fig. 4, which shows that the structure is nodular (2D) and closely packed columnar structure (3D) and the particle size distribution of the dust sample fraction respectively. The dry dust residues formed different shapes on the dust particle surfaces, evident in the three-dimensional image of the surface shown in Figure 8a. The texture height on the dust surface varies due to the dust residues, as observed from the linear scan of the removed dry dust from the surface (see Fig. 4 (b)). The particle size distribution of the dust sample fraction smaller than 140 nm was obtained using AFM analysis of the dust sample. Image analysis shows that the particle sizes range from 6nm to 100nm, as illustrated in Fig. 4 (c).

4. 3. Elements Analysis

A detailed examination of the EDX spectrum of coarse particles collected from storm dust and elements was observed. EDX carried out an elemental analysis of individual particles. Elemental composition reveals the ascendancy of Magnesium (Mg), Aluminum (Al), Silicon (Si), Calcium (Ca), Sulfur(S), Iron (Fe), Oxygen (O), Potassium (K), titanium (Ti), and sodium (Na) particles, as shown in Fig. 5. The presence of Si and O refers to the existence of Silica, which refers to earthy and sandy components that often result from the erosion of rocks. The western and northern regions of Iraq contain a high percentage of $CaCO_3$. In addition to C and O, Al and Si are significant contributors to

elemental composition, and it is generally accepted that about 72% of the Earth's crust consists of alumina silicates [28].

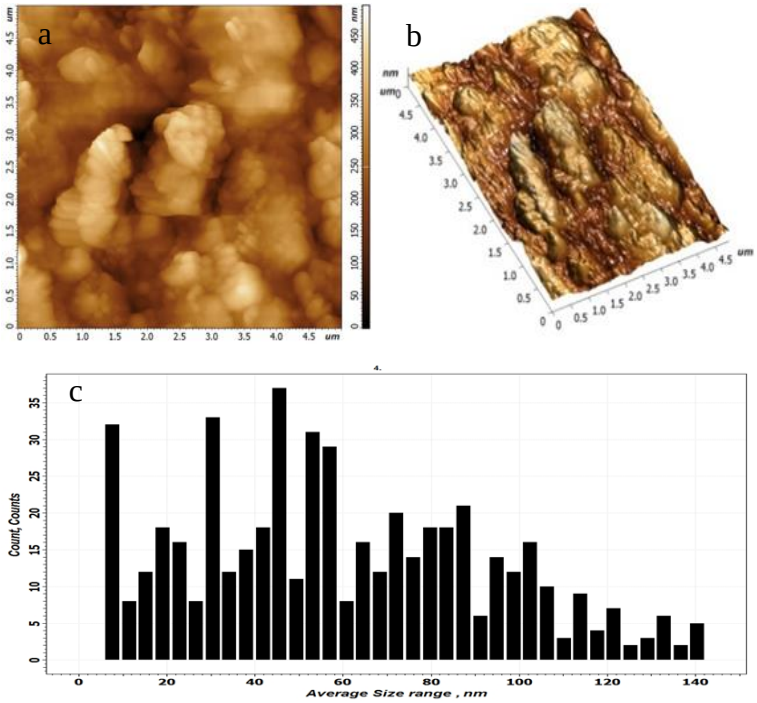

Figure 4: AFM image of dust sample showed (a) two-dimensional view (b) three-dimensional view (c) distribution of the dust sample practical size range.

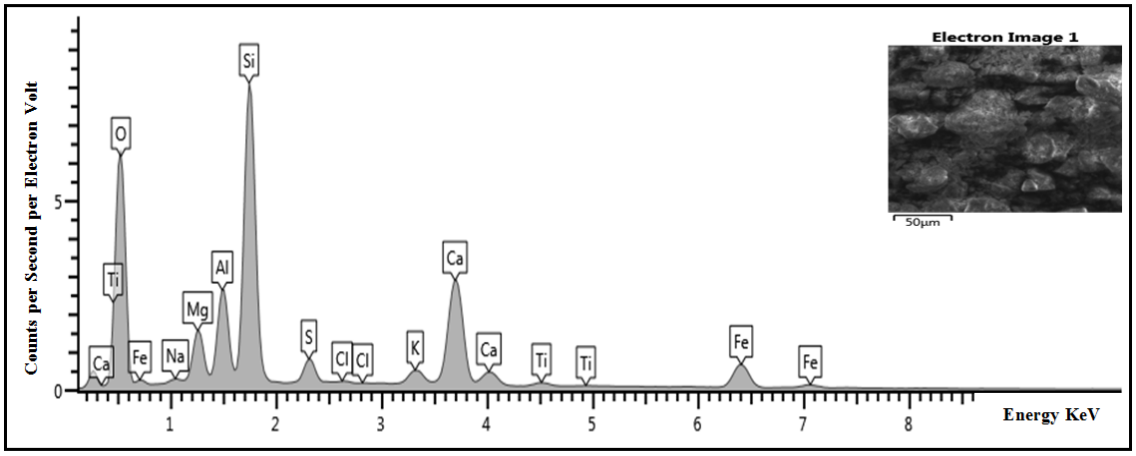

Figure 5: EDX spectrum of dust sample.

Iron May indicate the presence of minerals such as hematite and goethite, which add a red or brown color to the dust. Aluminum indicates the presence of clay minerals or feldspar, which are common in soil. Mg may indicate the presence of minerals such as dolomite or indicate marine sources. The ascendancy elemental composition of the dust sample is illustrated in Fig. 6. In this study, the concentrations of the elements in the dust storm sample were analyzed using XRF device and shows the number of oxides loaded by the severe dust storm that occurred in Iraq on May 16, 2022.

Table 2 presents the concentrations of the elements from sodium to uranium found in the dust storm samples in the current study, compared with findings from previous studies, and their background value in the earth’s crust.

The results of this study showed consistency with prior research in the concentrations of iron, cobalt, gallium, selenium, rubidium, strontium, tin, thorium, and barium, while the levels of nickel, germanium, molybdenum, tungsten, and mercury were higher. The concentration of heavy elements indicated that the regions exposed to the dust storm on May 16, 2022 are polluted with the heavy elements Ni, Co, Zn, As, Cd, Se, Sr, Mo, Sn, Ge, Te, Sb, Hg, Bi, Tl, and U.

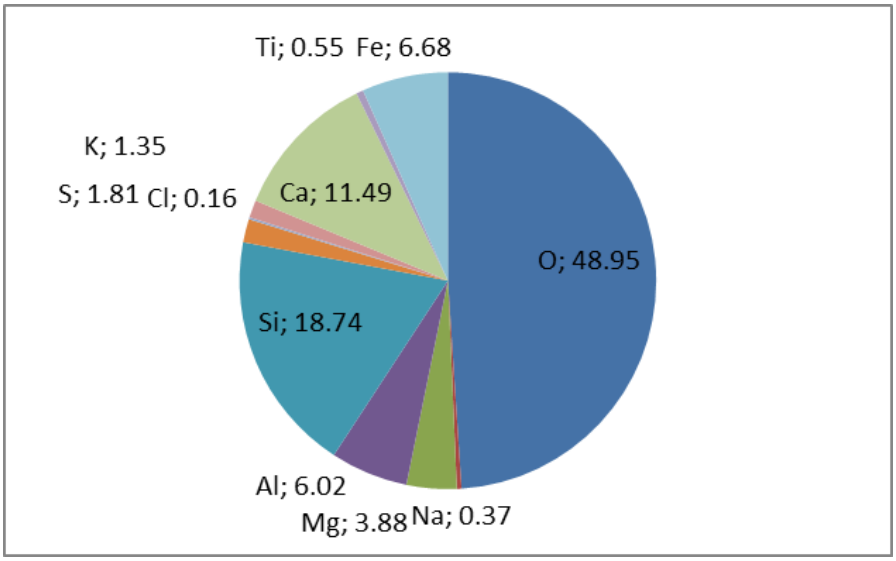

Figure 6: The ascendancy elemental composition of dust sample.

Table 2: The elements concentration measured in (ppm).

Element	Element name	Abundance in earth crust [29].	element concentration in this study	Attiya & Jones, (2020) [18].	Al-Dabbas et al., (2012) [29].	Kadhum, (2020) [21].	Al-Dabbas & Al-Khafaji, (2012) [30].	Aljewari & Al-Salman, (2023) [31]	Khwedi et al., (2022) [32].	Jaafar & Kadhum (2023) [33].
Na	Sodium	5800	2600	-	-	-	-	-	-	-
Mg	Magnesium	7900	390	-	-	-	-	-	-	-
Al	Aluminum	38200	2547	-	-	-	-	-	-	-
Si	Silicon	289000	22770	-	-	-	-	-	-	-
P	Phosphorus	1200	102.3	-	-	-	-	-	-	-
S	Sulfur	1200	5053	-	-	-	-	-	-	-
Cl	Chlorine	285	66.1	3689	-	-	-	-	-	-
K	Potassium	13400	6369	-	-	-	-	-	-	-
Ca	Calcium	53800	81830	-	-	-	-	-	-	-
Ti	Titanium	4758	1908	-	-	-	-	-	-	-
V	Vanadium	104.9	19	79	-	-	-	-	-	-
Cr	Chromium	80	245	-	-	-	-	-	10	7.47
Mn	Manganese	729	497	-	-	-	-	827.2	-	-
Fe	Iron	22300	31010	-	1100	-	648.5	54790	9400	-
Co	Cobalt	14.1	38.6	18.5	49	-	35.5	10	-	-
Ni	Nickel	33	322.5	62.5	131	106.4	128	-	45	17.381
Cu	Copper	60	25.5	51.5	53	-	34.5	49.3	6	11.737
Zn	Zinc	70	84.7	327	154	215.9	122.5	-	169	12.462
Ga	Gallium	16.2	9.6	8.5	-	-	-	-	-	-
Ge	Germanium	1.8	145	1.5	-	-	-	-	-	-

Table 3: (Continued.)

Element	Element name	Abundance in earth crust [29].	element concentration in this study	Attiya & Jones, (2020) [18].	Al-Dabbas et al., (2012) [29].	Kadhum, (2020) [21].	Al-Dabbas & Al-Khafaji, (2012) [30].	Aljewari & Al-Salman, (2023) [31]	Khwedi et al., (2022) [32].	Jaafar & Kadhum (2023) [33].
As	Arsenic	1.8	3.3	5	-	-	-	-	-	-
Se	Selenium	0.05	1.5	1	-	-	-	-	-	-
Br	Bromine	7	0.9	14.5	-	-	-	-	-	-
Rb	Rubidium	58	44.7	37	-	-	-	-	-	-
Sr	Strontium	375	537.8	501	-	-	-	-	-	-
Y	Yttrium	23.4	24.3	15	-	-	-	-	-	-
Mo	Molybdenum	2.4	32	1	-	-	-	-	-	-
Ag	Silver	0.37	4.6	-	-	-	-	-	-	-
Cd	Cadmium	0.5	4.3	-	27	1.33	14.5	2	-	0.42
Sn	Tin	2.5	6	6.5	-	-	-	-	-	-
Sb	Antimony	0.5	8	3	-	-	-	-	-	-
Te	Tellurium	0.005	13.7	-	-	-	-	-	-	-
I	Iodine	0.05	33.8	-	-	-	-	-	-	-
Ba	Barium	400	219	219	-	-	-	-	-	-
W	Tungsten	2.9	8.5	1	-	-	-	-	-	-
Hg	Mercury	0.08	7.9	2.5	-	-	-	-	-	-
Tl	Thallium	0.7	2.3	-	-	-	-	-	-	-
Pb	Lead	15	15.6	36.5	182	76.9	114.5	24.3	24	4.971
Bi	Bismuth	0.009	2.5	1	-	-	-	-	-	-
Th	Thorium	10	7.8	4.5	-	-	-	-	-	-
U	Uranium	2.5	3.2	1	-	-	-	-	-	-

An increase in the rates of Mg, Al, Si, Ca, S, Fe, and their oxides was observed in parts per million(ppm), which led to an increase in their oxides, respectively (MgO, Al_2O_3, SiO_2, CaO, SO_3, Fe_2O_3), as present in Table 3. The increase in these elements has a high environmental impact and health effects, as their accumulation in the earth's crust causes an increase in the concentrations of these elements.

Table 4: The elements oxide concentration measured in (ppm).

Element oxides	**conc. (ppm)**	**Element oxides**	**conc. (ppm)**	**Element oxides**	**conc. (ppm)**
Na_2O	3500	TiO_2	3184	ZnO	105.4
MgO	650	V_2O_5	35	As_2O_3	4.3
Al_2O_3	4813	Cr_2O_3	358	Rb_2O	48.9
SiO_2	48720	MnO	642	SrO	636
P_2O_5	235	Fe_2O_3	44340	SnO_2	7.6
SO_3	12620	CoO	49	BaO	244
K_2O	7672	NiO	410.5	WO_3	11
CaO	114500	CuO	32	PbO	16.8

To conduct mineral classification results based on EDX and XRF and determine the contents of different mineral types, we used the XRD technique to analyze the dust sample taken during a dust storm on May 16, 2022. The XRD result showed that the

samples contained the heavy elements indicated by XRF examination, which is consistent with the classification results based on EDX. The results of the X-ray diffraction of the dust sample revealed that it consists predominantly of clay minerals, with a lower proportion of recognized minerals and sand. The high levels of silt and clay in the dust are influenced by the exposure of sediments and rock formations to wind energy, which generates dust storms. Additionally, the origins of clay minerals are diverse.

4. 4. Results of Pollution Indicators

The concentrations of heavy elements are measured and compared with the natural abundance of elements in the earth's crust using three pollution indicators.

The CF index values for the elements (Ni, Ge, Se, Mo, Ag, Cd, Sb, Te, I, Hg, and Bi) showed very high pollution, while the elements (S, Cr, Tl) showed high pollution. The elements (Ca, Fe, Co, Zn, As, Sr, Y, Sn, W, Pb, U) have moderate pollution, while the elements (Mg, Na, Al, P, Si, K, Cl, Ti, Mn, V, Br, Cu, Ga, Ba, Rb, Th) have low pollution, see Table 4. The I-geo index showed extreme pollution of some heavy elements (Ge, Te, I, Hg, Bi, and Se) and severe pollution of the elements (Mo, Ag, Sb, Ni, and Cd). The elements (S, Cr, Tl) showed moderate pollution, and the elements (Ca, Co, As, Sn, W) were slightly polluted, while the other elements were practically unpolluted, as illustrated in Table 4.

The Pollution Load Index (PLI) for Pb, Ni, Cd, Zn, Cu, Cr, Hg, and Fe was calculated, and the samples were classified as deterioration on-site quality, indicating environmental pollution, where the PLI value was found to be equal to 2.68.

Table 5: CF, degree of contamination, and I-geo index of metals in dust storm sample.

Element	CF Range	Pollution description	Element	I-geo range	Pollution description
Ni	9.773	6≤ CF Very high contamination factor	Ge	5.747	5≤ I-geo Extremely polluted
Ge	80.556		Te	10.835	
Se	30.000		I	8.816	
Mo	13.333		Hg	6.041	
Ag	12.432		Bi	7.533	
Cd	8.600		Se	4.322	4≤ I-geo <5 Severely extremely polluted
Sb	16.000		Mo	3.152	3≤ I-geo <4 Severely polluted
Te	2740.000		Ag	3.051	
I	676.000		Sb	3.415	
Hg	98.750		Ni	2.704	2≤ I-geo <3 moderately severely polluted
Bi	277.778		Cd	2.519	
S	4.211	3≤ CF<6 Considerable contamination factor	S	1.489	1≤ I-geo <2 Moderately polluted
Cr	3.063		Cr	1.03	
Tl	3.286		Tl	1.131	
Ca	1.521	1≤ CF<3 Moderate contamination factor	Ca	0.02	0≤ I-geo <1 slightly polluted
Fe	1.391		Co	0.868	
Co	2.738		AS	0.29	
Zn	1.210		Sn	0.678	
AS	1.833		W	0.966	
Sr	1.434		Na	-1.743	I-geo <0 Practically unpolluted
Y	1.038		Mg	-4.925	
Sn	2.400		Al	-4.492	
W	2.931		Si	-4.251	
Pb	1.040		P	-4.137	

U	1.280		Cl	-2.693	
K	0.475	CF<1 Low contamination factor	K	-1.658	
Ti	0.401		Ti	-1.903	
Na	0.448		V	-3.05	
Mg	0.049		Mn	-1.138	
P	0.085		Fe	-0.109	
Cl	0.232		Cu	-1.819	
Cu	0.425		Zn	-0.31	
Ga	0.593		Ga	-1.34	
V	0.181		Br	-3.544	
Mn	0.682		Rb	-0.961	
Al	0.067		Sr	-0.0648	
Si	0.079		Y	-0.531	
Br	0.129		Ba	-1.454	
Ba	0.548		Pb	-0.528	
Rb	0.771		Th	-0.78	
Th	0.780		U	-0.229	

5. Conclusions

In this work, the primary dust storm sources were identified. The first source is from the shared border region between Syria (south of Rif-Dimasshq) and Jordan (north of Al-Ruwaished), and the second is from the northwestern areas of Iraq, specifically north of Anbar and south of Nineveh. Particle size analyses and X-ray diffraction specify that the dust samples are composed mostly of clay, sand, metals, fly ash, soot particles, natural organic ingredients, plant fibres, parts of seed husks, and tree leaves. The particles were sharp-edged and generally irregular, ranging from 6 nm to 50 µm. Increased concentrations of trace elements (Mg, Al, Si, Ca, S, and Fe) in dust storm samples negatively affect agriculture and plant health by inhibiting plant growth or causing death, impacting other organisms in the ecosystem, and potentially altering soil properties such as acidity. According to pollution indicators, the regions covered by the dust storm on May 16, 2022, are exposed to pollution with heavy elements (Ni, Co, Zn, As, Cd, Se, Sr, Mo, Sn, Ge, Te, Sb, Hg, Bi, Tl, and U), which have an environmental and health impact on the population, which increases as a result of the transfer of the dust mass loaded with heavy elements and oxides to the Iraqi regions from neighboring areas, according to the dust storm path. By using the CF indicator for elements (Pb, Ni, Cd, Zn, Cu, Cr, Hg, and Fe), the PLI value was found to be 2.68, indicating environmental pollution, and the samples were classified as deteriorating on-site quality.

Acknowledgments

We greatly appreciate the efforts of the following agencies: practical laboratories in the Scientific Research Authority /Directorate of Materials Research for analyzing the physical characterization and geochemical composition of dust samples, the National Aeronautics and Space Administration (NASA), and the European Organization for the Exploitation of Meteorological Satellites (EUMETSAT) for offering data on meteorological parameters.

Conflict of Interest

The author(s) declare that there is no conflict of interest.

References

1. N. Middleton and U. Kang, Sustainability **9**, 1053 (2017). https://doi.org/10.3390/su9061053.
2. A. P. Lisitzin, Russian Geol. Geophys. **52**, 1100 (2011). https://doi.org/10.1016/j.rgg.2011.09.006.

3. S. Nadimi, A. Ghanbarzadeh, A. Hassanpour, and A. Neville, Tribol. Int. **151**, 106433 (2020). https://doi.org/10.1016/j.triboint.2020.106433.
4. Y. Hao, Y. Gou, Z. Wang, W. Huang, F. Wan, M. Tian, and J. Chen, Atmosph. Res. **300**, 107215 (2024). https://doi.org/10.1016/j.atmosres.2023.107215.
5. Y. Wang, C. Zhao, D. Dong, and K. Wang, Ecol. Indicat. **151**, 110302 (2023). https://doi.org/10.1016/j.ecolind.2023.110302.
6. F. A. L. Pacheco, R. M. B. Santos, L. F. Sanches Fernandes, M. G. Pereira, and R. M. V. Cortes, Sci. Tot. Envir. **537**, 421 (2015). https://doi.org/10.1016/j.scitotenv.2015.07.127.
7. H. Shen, J. Abuduwaili, A. Samat, and L. Ma, Arabian J. Geosci. **9**, 625 (2016). https://doi.org/10.1007/s12517-016-2646-9.
8. S. M. Awadh, Atmosphere **14**, 180 (2023). https://doi.org/10.3390/atmos14010180.
9. J. F. Kok, T. Storelvmo, V. A. Karydis, A. A. Adebiyi, N. M. Mahowald, A. T. Evan, C. He, and D. M. Leung, Nat. Rev. Earth Envir. **4**, 71 (2023). https://doi.org/10.1038/s43017-022-00379-5.
10. A. F. Stein, R. R. Draxler, G. D. Rolph, B. J. B. Stunder, M. D. Cohen, and F. Ngan, Bullet. American Meteorolog. Soci. **96**, 2059 (2015). https://doi.org/10.1175/BAMS-D-14-00110.1.
11. R. R. Ismail, S. H. Halos, and B. Q. Al-Abudi, Kuwait J. Sci. **52**, 100328 (2025). https://doi.org/10.1016/j.kjs.2024.100328.
12. T. Rajaee, N. Rohani, E. Jabbari, and B. Mojaradi, Arabian J. Geosci. **13**, 461 (2020). https://doi.org/10.1007/s12517-020-05443-2.
13. A. Ali, N. Zhang, and R. M. Santos Appl. Sci., 2023. **13**, 1260. https://doi.org/10.3390/app132312600.
14. M. Chaupard, M. De Frutos, and R. Gref, Part. Part. Syst. Charact. **38**, 2100022 (2021). https://doi.org/10.1002/ppsc.202100022.
15. N. Joudeh and D. Linke, J. Nanobiotech. **20**, 262 (2022). https://doi.org/10.1186/s12951-022-01477-8.
16. A. Venkateshaiah, V. V. T. Padil, M. Nagalakshmaiah, S. Waclawek, M. Černík, and R. S. Varma, Polymers **12**, 512 (2020). https://doi.org/10.3390/polym12030512.
17. A. F. Marsala, T. Loermans, S. Shen, C. Scheibe, and R. Zereik, *Real-Time Mineralogy, Lithology, and Chemostratigraphy While Drilling Using Portable Energy-Dispersive X-Ray Fluorescence*, *SPE EUROPEC/EAGE Annual Conference and Exhibition*. 2011, OnePetro: Vienna, Austria. pp. SPE.
18. A. A. Attiya and B. G. Jones, SN Appl. Sci. **2**, 1614 (2020). https://doi.org/10.1007/s42452-020-03326-5.
19. J. Qin, C. Yang, C. Cui, J. Huang, A. Hussain, and H. Ma, J. Envir. Sci. **47**, 91 (2016). https://doi.org/10.1016/j.jes.2016.03.013.
20. N. Q. Kadhem, I. F. Hussein, and B. A. Hussain, J. Phys.: Conf. Ser. **2857**, 012049 (2024). https://doi.org/10.1088/1742-6596/2857/1/012049.
21. S. A. Kadhum, Envir. Sci. Pollut. Res. Int. **27**, 8570 (2020). https://doi.org/10.1007/s11356-019-07380-4.
22. L. H. Kamel, M. B. Mahmood, and S. K. Al-Zurfi, Iraqi J. Sci. **64**, 1093 (2023). https://doi.org/10.24996/ijs.2023.64.3.6.
23. H. Haghnazar, S. Soltani-Gerdefaramarzi, M. Ghasemi, and K. H. Johannesson, Envir. Earth Sci. **82**, 316 (2023). https://doi.org/10.1007/s12665-023-11000-3.
24. Eumetsat. *Satellite Data from Severi on the Meteosat Second Generation Satellite*; https://view.eumetsat.int/productviewer?v=default.
25. A. Bhattacharjee, H. Mandal, M. Roy, J. Kusz, and W. Hofmeister, J. Magnet. Magnet. Mat. **323**, 3007 (2011). https://doi.org/10.1016/j.jmmm.2011.06.036.
26. H. W. Samuelson, A. Lantz, and C. F. Reinhart, Build. Envir. **54**, 71 (2012). https://doi.org/10.1016/j.buildenv.2012.02.001.
27. R. Senthil Kumar and P. Rajkumar, Infra. Phys. Tech. **67**, 30 (2014). https://doi.org/10.1016/j.infrared.2014.06.002.
28. B. Bahadar Zeb, K. Khan Alam, A. Armin Sorooshian, T. Blaschke, I. Ahmad, and I. Shahid, Aero. Air Qual. Res. **18**, 1431 (2018). https://doi.org/10.4209/aaqr.2017.09.0340.
29. W. Joint and W. H. Organization, *Health Risks of Heavy Metals from Long-Range Transboundary Air Pollution* (Europe, World Health Organization, 2007).
30. M. Al-Dabbas and R. Al-Khafaji, Iraqi J. Sci. **53**, 57 (2024). https://doi.org/10.24996/ijs.2012.53.Remote%20Sensing-Conf.%25g.
31. A. F. M. Aljewari and I. M. A. Al-Salman, Ibn AL-Haitham J. Pure Appl. Sci. **36**, 1 (2023). https://doi.org/10.30526/36.1.2973.
32. K. Khwedim, M. T. Ahmed, and M. A. Najemalden, Iraqi J. Sci. **63**, 3817 (2022). https://doi.org/10.24996/ijs.2022.63.9.14.
33. B. I. Jaafar and S. A. Kadhum, IOP Conf. Ser. Earth Envir. Sci. **1259**, 012040 (2023). https://doi.org/10.1088/1755-1315/1259/1/012040.

تقييم التلوث بالعناصر الثقيلة والتأثيرات البيئية للعاصفة الغبارية الشديدة في العراق في آيار 2022

رفاه رشيد اسماعيل[1]، سعدية حسن هلوس[2]، بشرى قاسم العبودي[1]
[1]قسم الفلك والفضاء، كلية العلوم، جامعة بغداد، بغداد، العراق
[2]قسم علوم الجو والفضاء، مركز بحوث وتكنولوجيا الفضاء، هيئة البحث العلمي، بغداد، العراق

الخلاصة

يمكن أن يكون للعواصف الغبارية المتكررة في العراق عواقب بعيدة المدى على توزيع ووفرة العناصر الثقيلة والعناصر النزرة داخل التربة، مما يؤثر في نهاية المطاف على ديناميكية النظم البيئية. تهدف هذه الدراسة إلى تحديد مصادر العاصفة الغبارية الشديدة في العراق في 16 مايو 2022، وتقييم تلوث العناصر الثقيلة وتأثيراتها البيئية. كشفت النتائج أن مسار نموذج HYSPLIT للعاصفة الغبارية يتفق مع صور المتحسس MODIS. تم تحديد مصادر العاصفة الغبارية. كان هناك مصدرين للعاصفة الغبارية، الأول اقليمي من منطقة الحدود المشتركة بين سوريا (جنوب ريف دمشق) والأردن (شمال الرويشد)، والثاني محلي من المناطق الشمالية الغربية من العراق، وتحديدًا شمال الأنبار وجنوب نينوى. تتكون عينات الغبار في الغالب من الطين والرمل والمعادن، وفقًا لتحليلات حجم الجسيمات، تتراوح احجام الجسيمات من 6 نانومتر إلى 50 مايكرومتر. لوحظ زيادة تركيزات العناصر النزرة، والتي تؤثر في النظام البيئي، بالإضافة إلى إمكانية تغيير خصائص التربة. كذلك هناك زيادة في تركيز المعادن الثقيلة والتي تؤثر سلبا على البيئة وصحة الإنسان، حيث أظهرت قيم معامل التلوث تلوثا عاليا جدا للعناصر(Ni, Ge, Se, Mo, Ag, Cd, Sb, Te, I, Hg, Bi) ، في حين أشار مؤشر I-geo إلى تلوثه الشديد ببعض العناصر الثقيلة (Ge, Te, I, Hg, Bi, Se).وباستخدام قيم معامل التلوث للعناصر (Pb, Ni, Cd, Zn, Cu, Cr, Hg, Fe) وجد أن قيمة مؤشر حمل التلوث 2.68 مما يدل على وجود تلوث بيئي.

الكلمات المفتاحية: العواصف الغبارية، التأثيرات البيئية، مؤشرات التلوث، العناصر الثقيلة، العناصر النزرة.